Uncertainties in using the hodograph method to retrieve gravity wave characteristics from individual soundings

Fuqing Zhang and Shuguang Wang
Department of Atmospheric Sciences, Texas A&M University, College Station, Texas, USA

Riwal Plougonven
National Center for Atmospheric Research, Boulder, Colorado, USA

Received 27 February 2004; revised 5 May 2004; accepted 14 May 2004; published 11 June 2004.

[1] The hodograph method is commonly used to retrieve inertio-gravity wave characteristics from individual vertical profiles of the winds. In order to estimate the uncertainties of this method, we have analyzed mesoscale numerical simulations of a gravity wave event in which a coherent quasi-monochromatic inertio-gravity wave packet is present. Single profiles are extracted from the simulations, analyzed using the hodograph method, and the derived wave characteristics are compared to the reference values determined from the four-dimensional simulated fields. Although the conditions favor the use of the hodograph method, the derived wave parameters possess significant uncertainties. *INDEX TERMS:* 3329 Meteorology and Atmospheric Dynamics: Mesoscale meteorology; 3334 Meteorology and Atmospheric Dynamics: Middle atmosphere dynamics (0341, 0342); 3362 Meteorology and Atmospheric Dynamics: Stratosphere/troposphere interactions; 3384 Meteorology and Atmospheric Dynamics: Waves and tides; 3394 Meteorology and Atmospheric Dynamics: Instruments and techniques; *KEYWORDS:* Gravity waves, radiosonde, hodograph method. **Citation:** Zhang, F., S. Wang, and R. Plougonven (2004), Uncertainties in using the hodograph method to retrieve gravity wave characteristics from individual soundings, *Geophys. Res. Lett.*, *31*, L11110, doi:10.1029/2004GL019841.

1. Introduction

[2] The hodograph method [*Sawyer*, 1961] is based on the linear theory of gravity waves in a fluid at rest, or in a uniform flow. The method allows to identify low-frequency waves ($\omega < 10f$, where f is the Coriolis parameter) and has been used in a considerable number of observational studies [e.g. *Wang and Geller*, 2003; *Plougonven et al.*, 2003]. However, it appears that the uncertainties associated with this method have not received sufficient attention. Uncertainties may be introduced by interpreting, using linear theory, wave signals for which the dynamics is nonlinear, or has to be linearized about a more complex flow than a uniform flow. The differences in the dynamics of the waves can for instance be due to the effect of vertical shear [*Kunze*, 1985; *Hines*, 1989; *Thomas et al.*, 1999], or horizontal shear [*Kunze*, 1985]. Uncertainties can also be introduced if the sounding profiles (radiosondes or dropsondes) are interpreted as instantaneous vertical profiles of the wind and temperature. In reality, the radiosonde takes time to ascend and drifts horizontally as it ascends. The uncertainty associated with the finite ascent rate has been addressed in several previous studies [e.g., *Guest et al.*, 2000] and will not be addressed further.

[3] In this study, we will try to access potential uncertainties in using the hodograph method to retrieve gravity wave characteristics even if the wave packet can be reasonably approximated by linear analysis. These uncertainties may be due to: (1) the separation into a background flow and a perturbation, since there is unavoidably some arbitrariness in the choice of the filter or polynomial fit used for that purpose; (2) the geographical variation of the wave packet; and (3) the presence of multiple waves. We estimate the importance of these uncertainties in a case study, using high-resolution numerical simulations in which a coherent quasi-monochromatic low-frequency wave is present. The reference characteristics of the wave are obtained from the overall 4-dimensional (4D) output of the simulations. Characteristics retrieved from individual profiles of the simulated wind by the hodograph method are then compared with those from 4D output.

2. Experimental Design and the Control Simulations

[4] We will first use a state-of-the-art mesoscale model to simulate a gravity wave event that occurred on 5–6 February 1997 during the Fronts and Atlantic Storm-Tracks Experiment, and which has been investigated in a recent paper by *Plougonven and Teitelbaum* [2003] (hereinafter referred to as PT) using radiosonde observations.

[5] The mesoscale model MM5 is employed for the simulations. MM5 has been demonstrated to be capable of simulating realistic gravity waves associated with baroclinic jet-front systems in many previous studies [e.g., *Zhang et al.*, 2001]. We have performed two experiments with effective horizontal grid spacing 30 and 10 km, respectively. The 30-km simulation ("EXP30KM") employs only one model domain (D1) with 190 × 130 horizontal grid points and 60 vertical layers with vertical grid spacing of 314 m. The 10-km simulation ("EXP10KM") employs two model domains with D1 the same as in EXP30KM except that 90 vertical layers are used with vertical grid spacing of 262 m. The 10-km nested domain (D2) employs 240 × 180 horizontal grid points. The ECMWF analysis is used to provide the initial and boundary conditions for the MM5 simulations. The simulation is initialized at 0000 UTC

0094-8276/04/2004GL019841$05.00

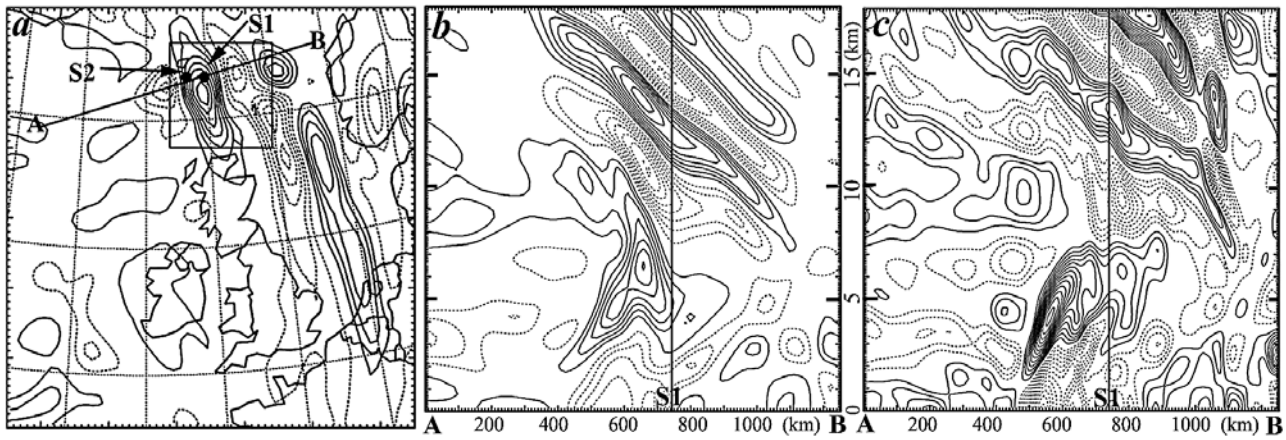

Figure 1. (a) Map of the horizontal divergence (every 2.0×10^{-5} s^{-1}) on isobaric surface of 158 hPa from EXP30KM valid at 00Z 6 Feb 2000; latitude and longitude are plotted every 5 degrees. (b–c) Cross sections of the horizontal divergence (every 2.0×10^{-5} s^{-1}) along line AB denoted in (a) from (b) EXP30KM and (c) EXP10KM, respectively.

5 February 1997, a day before the gravity waves of interest in this study appear, and is integrated for 36 h.

[6] The large-scale simulations from both EXP30KM and EXP10KM verified well against the ECMWF analysis throughout the 36-h model integration (not shown). In particular, they both simulated well the strength and location of the upper-tropospheric jet streak just upstream of a geopotential ridge in the northern Atlantic Ocean southeast of Greenland and west of the British Isles (see Figure 1 of PT). This flow configuration is conducive to gravity wave generation, as shown by *Uccellini and Koch* [1987] and *Zhang* [2004]. In the vicinity and downstream of this jet streak, strong gravity wave activity has indeed been detected in the observational study of PT. Inertio-gravity waves in this region of the flow are found in both EXP30KM and EXP10KM in maps of the divergence (alternating bands of convergence and divergence; Figure 1a), as well as in wind and temperature fluctuations. These are consistent with the waves described in PT from the ECMWF analyses (see Figure 2c of PT), which were themselves in qualitative agreement with the observations. As in the ECMWF analysis, these gravity waves are propagating east and northeastward relative to the ground. The magnitudes of the wind and temperature perturbations (with maxima of 10 ms^{-1} and 5 K, respectively) also compared well. The horizontal wavelengths of these waves (slightly shorter than in ECMWF analyses) are approximately 300–500 km from EXP30KM with shorter wavelengths to the west and north side of the wave packet. A cross section of the horizontal divergence along the propagation vector (line AB) of the northern wave packet is displayed in Figure 1b for EXP30KM and Figure 1c for EXP10KM, respectively.

[7] We first derive reference values for the gravity wave characteristics by examining the 4D output of the MM5 simulations. This direct estimation of the wave characteristics will then be compared with estimates obtained from individual soundings from the model, using the hodograph method and different polynomial fits. The vertical wavelength (λ_z) in EXP30KM (Figures 1a and 1b) is estimated as twice the distance between the maximum and minimum divergence (between 12 and 15 km) is ~5.2 km. The horizontal wavelength (λ_H) at 158 hPa (~13 km) along cross section AB is approximately 310 km (with variations of less than 10%). The ground-based phase speed of this wave packet averaged between 2200 UTC 5 and 0200 UTC 6 February is ~15 ms^{-1} east-northeastward (propagation direction $\varphi = 16.7°$). The background horizontal wind speed

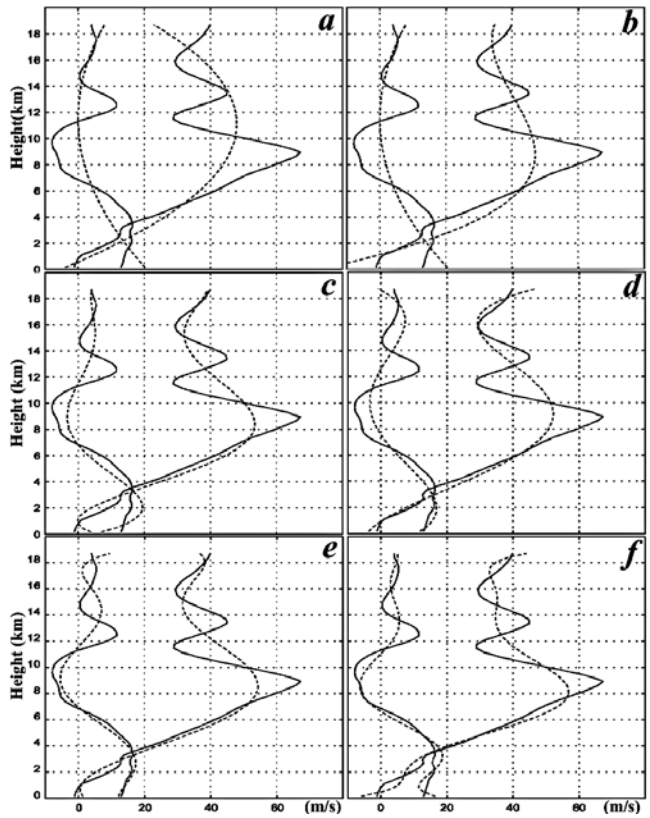

Figure 2. Vertical profiles (solid) of horizontal winds at sounding S1 (denoted in Figure 1) from EXP30KM and the background profiles for different orders [(a)2nd, (b) 3rd, (c) 4th, (d) 5th, (e) 6th and (f) 7th] of polynomial fit (dashed).

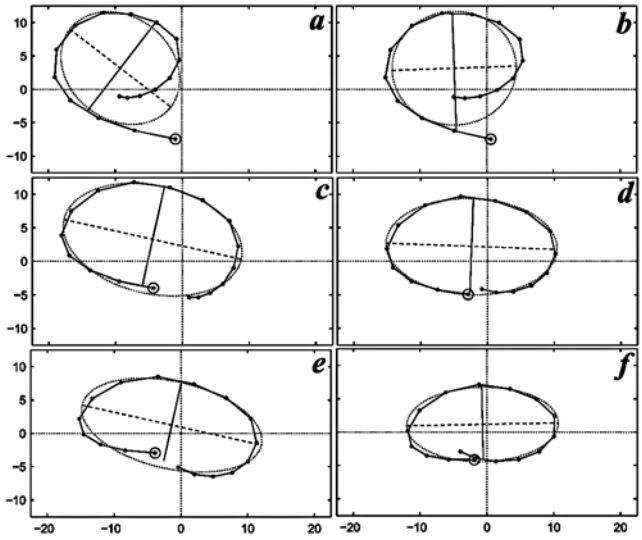

Figure 3. Hodographs of sounding S1 (denoted in Figure 1) from EXP30KM with different orders [(a) 2nd, (b) 3rd, (c) 4th, (d) 5th, (e) 6th and (f) 7th] of polynomial fit. The altitudes of the starting point (denoted with an open circle) and the end point are 10.2 and 15.6 km, respectively. Major (minor) axes of the elliptical fit are denoted with dashed (solid) lines. Dots are every 314 m.

(U) valid at 00Z 6 February averaged between 10 and 16 km is 35 ms^{-1}. The intrinsic phase speed estimated directly from the model output is thus ~ -20 ms^{-1}, propagating against the background flow. With the Coriolis parameter (f) equal to 1.25×10^{-4} s^{-1} at this latitude and the buoyancy frequency (N) equal to 0.02 s^{-1}, the intrinsic wave speed (c_i) estimated independently from the linear dispersion relationship ($c_i = \frac{\omega_i}{k} = -\sqrt{\frac{f^2}{k^2} + \frac{N^2}{m^2}}$) is ~ -17.7 ms^{-1}(with intrinsic frequency $\omega_i \sim 3f$). This derived value compares well with the intrinsic phase speed measured from the model (~ -20.0 ms^{-1}). Thus, the 30-km MM5 simulation (EXP30KM) produces a clearly defined, intense and mostly monochromatic inertio-gravity wave (IGW) packet, and the characteristics of this inertio-gravity wave packet are consistent with linear theory.

[8] In the higher-resolution EXP10KM, a primary wave with characteristics similar to those in EXP30KM described above is also simulated. However, waves with shorter wavelengths, superposed on the primary wave, are present as well in EXP10KM (Figure 1c). Multiple waves are likely to be present in the real atmosphere. Uncertainties in the characteristics of the gravity waves generated in these high-resolution simulations will be examined in the following section.

3. Uncertainties in Hodograph Method

[9] In this section, we will attempt to access the uncertainties of the commonly-used hodograph method when used on individual sounding profiles to retrieve the gravity wave characteristics. We restrict our analyses to true vertical profiles derived from the MM5 output valid at 0000 UTC 6 February. We apply polynomial fits of 6 different orders (2nd, 3rd, 4th, 5th, 6th and 7th) from the sea-level to 18 km to separate each sounding profile into a mean and a perturbation for the zonal and meridional winds and for temperature (similar uncertainties are also found when applying the filters to a shorter segment of the soundings or when a different filter is used). Vertical profiles of sounding S1 (denoted in Figure 1) from EXP30KM and different orders of polynomial fit are displayed in Figure 2. The hodographs of the perturbation winds for this sounding are plotted in Figure 3. An elliptical fit from 10.2 and 15.6 km has been used to determine the major/minor axis in these hodographs. Following linear theory [*Gill*, 1982], the ratio between the major and minor axes of the fitted ellipse is then used to determine the intrinsic frequency ($\omega_i = \sqrt{f^2 + \frac{k^2N^2}{m^2}}$). The orientation of the major axis determines the wave propagation direction. For consistency with the direct estimation from the 4D output, the vertical wavelength is estimated as twice the distance in height between the ends of the minor axis (solid line). Thus, the horizontal wavelength can be determined from the linear dispersion relationship. The same method of analysis is also applied to another sounding S2 (also denoted in Figure 1). Wave characteristics derived from these two soundings and their comparison to the reference values derived from the 4D model output are summarized in Table 1.

[10] Figures 2–3 and Table 1 revealed large variations (uncertainties) of all the wave characteristics estimated through the hodograph method. The uncertainties first come from the arbitrariness in choosing polynomial fits of different orders to separate wave perturbations from a background flow (Figure 2). For example, the horizontal wavelength for S1 differs by a factor of 3–4 from the 3rd to the 7th order estimate; the intrinsic frequency estimate for S2 differs by a factor of 2 from the 3rd order to the 6th order polynomial fit. Consequently, one may expect even larger uncertainties in quantities estimated after further assumptions, such as momentum fluxes.

[11] Among all the estimates from these two nearby sounding profiles with different polynomial fits, all have,

Table 1. Comparisons of Wave Parameters Derived from EXP30KM[a]

		Sounding 1 (S1)						Sounding 2 (S2)					
	4D	2nd	3rd	4th	5th	6th	7th	2nd	3rd	4th	5th	6th	7th
ω_i ($10^{-4}s^{-1}$)	4.05	1.6	1.4	2.1	2.3	2.6	2.6	2.2	2.0	3.2	2.7	4.1	2.9
c_i (ms^{-1})	20	22.9	32.8	18.4	18.0	20.6	17.6	21.8	23.1	20.2	19.7	18.6	18.3
φ(°)	16.7	−37.6	2.0	−12.7	−2.1	−12.6	1.1	−16.3	−12.9	−6.0	2.4	0.3	3.6
λ_z (km)	5.2	4.1	4.0	4.7	4.6	5.8	4.7	5.7	5.6	5.8	5.4	5.6	5.1
λ_H (km)	310	899	1473	551	491	498	426	624	716	396	458	285	397

[a]Symbols denoted for wave characteristics are defined in the text.

Table 2. Estimate of The Horizontal (Vertical) Wavelengths in km Derived from 16 Individual Soundings in EXP30KM Located in the Square Box Denoted in Figure 1a

132 (4.9)	445 (3.3)	NA	333 (5.7)
420 (6.5)	**498 (5.8)**	1480 (8.5)	229 (2.7)
729 (7.1)	306 (4.6)	408 (3.6)	218 (1.8)
604 (3.8)	604 (5.6)	1040 (4.6)	NA

at least for one wave parameter, significant differences with the reference values derived from the 4D model output. There is a general tendency that higher-order filters appear to give better estimate with the 6th order fitting of S2 the closest to the estimate from the 4D model output. The magnitude of the uncertainties varies for different aspects of the wave characteristics: estimate of the vertical wavelength and intrinsic phase speed in general are more accurate than that of the intrinsic frequency or horizontal wavelength. The horizontal wavelength is very sensitive to the aspect ratio, particularly for low-frequency waves. It is worth pointing out that all the wave propagation direction estimates are biased systematically toward the right compared to the direct 4D estimates, possibly due to varying background winds.

[12] Uncertainties also come from the location of the soundings: the same 6th fitting gives sharply different estimates for the two soundings located apart merely by 1/4 of the horizontal wavelength. The uncertainty due to the location of the sounding is further illustrated in Table 2, which shows the distribution of the horizontal wavelength estimated from 16 individual soundings in the vicinity of the same wave packet with the same 6th order filter. These soundings are equally spaced (every 150 km by 150 km) in the square box indicated in Figure 1a. Estimates for two of the soundings, both on the edge of the wave packet, are not given ("NA") because they do not possess clear signals of IGWs. The values of the S1 sounding are denoted in bold numbers.

[13] There are even larger uncertainties in using the hodograph method when multiple waves are present, as is the case in the higher resolution simulation of EXP10KM (Figure 1c). Roughly speaking, the primary gravity wave produced in the higher resolution simulation (EXP10KM) coincides well with those from EXP30KM (Figure 1b vs. Figure 1c). Wave characteristics derived directly from the 4D model output of EXP10KM (as shown in Table 3) are very similar to those in EXP30KM except for slightly larger vertical wavelength. The hodographs between 10.2 and 15.6 km for sounding S1 (its location denoted in Figure 1c) for EXP10KM are plotted in Figure 4. Wave characteristics derived from this sounding are summarized in Table 3.

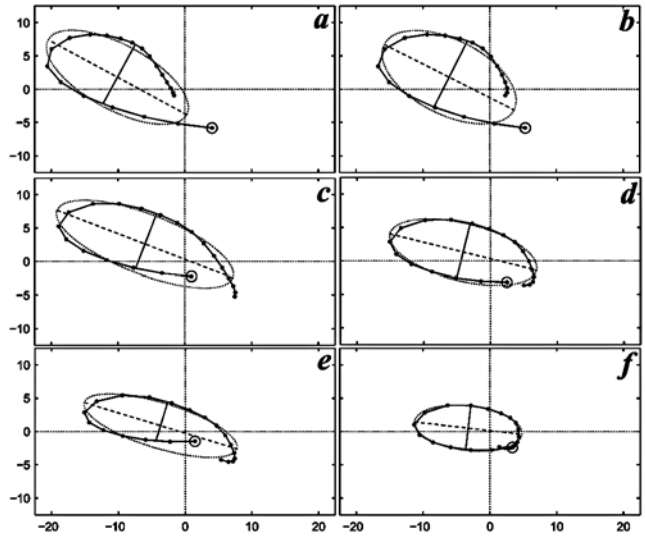

Figure 4. As in Figure 3 except for hodographs of sounding S1 from EXP10KM. Dots are every 262 m.

[14] As in EXP30KM, all the hodographs indicate strong presence of inertial gravity waves. However, though the primary wave looks similar from the direct model output in Figures 4c and 4d, no set of estimates in Table 3 compared systematically well with those in Table 1. The uncertainties in the vertical wavelength are larger. In contrast with the estimates from EXP30KM, the intrinsic frequencies have a bias toward higher frequencies than the reference value. Consequently, the uncertainties on the horizontal wavelength are here again large (values varying within a factor 2), but they are generally closer to the reference value.

4. Concluding Remarks

[15] We have compared, in high-resolution numerical simulations, gravity wave characteristics derived from vertical profiles using the hodograph method with reference values obtained from the full 4D output of the simulations. Although the primary wave present in the simulations was well described by linear theory, important uncertainties were found to exist for all the wave characteristics derived from single vertical profiles using the hodograph method. Both the vertical wavelength and the intrinsic frequency were very sensitive to the filter used to separate the wave from a background flow. As a result, large uncertainties were found in the estimates of the horizontal wavelength (smaller uncertainties are expected for waves with shorter vertical wavelength when the scale separation between the gravity waves and the background flow is more pronounced). One

Table 3. Comparisons of Wave Parameters Derived from EXP10KM

		Sounding 1 (S1)						Sounding 2 (S2)					
	4D	2nd	3rd	4th	5th	6th	7th	2nd	3rd	4th	5th	6th	7th
ω_i (10^{-4} s^{-1})	4.05	5.0	3.8	5.0	3.7	6.9	3.9	5.0	3.8	5.0	3.7	6.9	3.9
c_i (ms^{-1})	20.0	12.4	13.6	11.0	25.6	19.9	24.5	23.8	23.9	20.0	20.7	15.7	15.6
φ(°)	16.7	−28.4	−26.8	−21.0	−13.9	−16.9	−6.6	−19.6	−22.7	−17.2	−15.6	−9.7	−0.8
λ_z (km)	5.5	3.8	4.0	3.3	7.5	6.2	7.3	7.2	7.1	6.1	6.1	4.8	4.6
λ_H (km)	310	156	225	138	436	181	392	298	394	250	352	143	249

interesting point to note was a systematic bias in the estimated direction of the wave-vector, likely due to the background winds, which could be of importance for estimates of the momentum fluxes. Finally, although the wave packet appears well-defined over a broad region of space, the spatial variations of the wave characteristics estimated from soundings in various locations were very large. This would make it difficult to reconstruct the extent of this wave packet even from a dense network of individual soundings.

[16] **Acknowledgments.** We benefited from discussions with Todd Lane, Craig Epifanio and Andreas Dörnbrack. This research was supported by NSF Grant ATM-0203238.

References

Gill, A. E. (1982), *Atmospheric-Ocean Dynamics*, 662 pp., Academic, San Diego, Calif.

Guest, F., M. Reeder, C. Marks, and D. Karoly (2000), Inertia-gravity waves observed in the lower stratosphere over Macquarie Island, *J. Atmos. Sci.*, *57*, 737–752.

Hines, C. (1989), Tropopausal mountain waves over Arecibo: A case study, *J. Atmos. Sci.*, *46*, 476–488.

Kunze, E. (1985), Near-inertial wave propagation in geostrophic shear, *J. Phys. Oceanogr.*, *15*, 544–565.

Plougonven, R., and H. Teitelbaum (2003), Comparison of a large-scale inertia-gravity wave as seen in the ECMWF analyses and from radiosondes, *Geophys. Res. Lett.*, *30*(18), 1954, doi:10.1029/2003GL017716.

Plougonven, R., H. Teitelbaum, and V. Zeitlin (2003), Inertia gravity wave generation by the tropospheric midlatitude jet as given by the Fronts and Atlantic Storm-Track Experiment radio soundings, *J. Geophys. Res.*, *108*(D21), 4686, doi:10.1029/2003JD003535.

Sawyer, J. S. (1961), Quasi-perodic wind variations with height in the lower stratosphere, *Q. J. R. Meteorol. Soc.*, *87*, 24–33.

Thomas, L., R. M. Worthington, and A. J. McDonald (1999), Inertia-gravity waves in the troposphere and lower stratosphere associated with a jet stream exit region, *Ann. Geophys.*, *17*, 115–121.

Uccellini, L. W., and S. E. Koch (1987), The synoptic setting and possible source mechanisms for mesoscale gravity wave events, *Mon. Weather Rev.*, *115*, 721–729.

Wang, L., and M. A. Geller (2003), Morphology of gravity-wave energy as observed from 4 years (1998–2001) of high vertical resolution U.S. radiosonde data, *J. Geophys. Res.*, *108*(D16), 4489, doi:10.1029/2002JD002786.

Zhang, F. (2004), Generation of mesoscale gravity waves in the upper-tropospheric jet-front systems, *J. Atmos. Sci.*, *61*, 440–457.

Zhang, F., S. E. Koch, C. A. Davis, and M. L. Kaplan (2001), Wavelet analysis and the governing dynamics of a large-amplitude gravity wave event along the east coast of the United States, *Q. J. R. Meteorol. Soc.*, *127*, 2209–2245.

R. Plougonven, National Center for Atmospheric Research, P. O. Box 3000, Boulder, CO 80307-3000, USA.

S. Wang and F. Zhang, Department of Atmospheric Sciences, Texas A&M University, MS 3150, College Station, TX 77843-3150, USA. (fzhang@tamu.edu)